Feasibility evaluation of middle-phase ^{18}F-florbetaben positron emission tomography imaging using centiloid quantification and visual assessment

Cheng-Han Wu[1], Yueh-Hsun Lu[1,2,3], Tse-Hao Lee[4], Chun-Yuan Tu[5,6], Jong-Ling Fuh[3,7], Yuh-Feng Wang[4,5], Bang-Hung Yang[4,8]

[1]Department of Radiology, Taipei Medical University-Shuang Ho Hospital, New Taipei; [2]Department of Radiology, School of Medicine, College of Medicine, Taipei Medical University, Taipei; [3]School of Medicine, National Yang Ming Chiao Tung University, Taipei; [4]Department of Nuclear Medicine, Taipei Veterans General Hospital, Taipei; [5]Department of Medical Imaging and Radiological Technology, Yuanpei University of Medical Technology, Hsinchu; [6]Association of Medical Radiation Technologists, Taipei; [7]Department of Neurology, Neurological Institute, Taipei Veterans General Hospital, Taipei; [8]Department of Biomedical Imaging and Radiological Sciences, National Yang Ming Chiao Tung University, Taipei

Contributions: (I) Conception and design: CH Wu, BH Yang, CY Tu; (II) Administrative support: BH Yang, YH Lu, YF Wang; (III) Provision of study materials or patients: BH Yang, JL Fuh; (IV) Collection and assembly of data: CH Wu, BH Yang; (V) Data analysis and interpretation: CH Wu, BH Yang, TH Lee, CY Tu; (VI) Manuscript writing: All authors; (VII) Final approval of manuscript: All authors.

Correspondence to: Bang-Hung Yang, PhD. Adjunct Associate Professor, Department of Nuclear Medicine, Taipei Veterans General Hospital, No. 201, Sec. 2, Shipai Rd., Beitou District, Taipei 112. Email: bhyang@vghtpe.gov.tw; Chun-Yuan Tu, PhD. Assistant Professor, Department of Medical Imaging and Radiological Technology, Yuanpei University of Medical Technology, No. 306, Yuanpei Street, Hsinchu 300. Email: yuan110072@mail.ypu.edu.tw.

Background: ^{18}F-florbetaben (FBB) positron emission tomography (PET) scan has been widely used in research and routine clinical practice. Most studies used late-phase (scanning from 90 to 110 min after injection) FBB scans to generate beta-amyloid accumulation data. The feasibility of middle-phase scan is seldom discussed. Using the middle-phase data can shorten the patients' waiting between the injection and scan, and hospital can acquire more flexible schedule of routine scan.

Methods: Paired middle-phase (60–80 min) FBB scans and standard (90–110 min) FBB scans were obtained from 27 subjects (12 neurodegenerative dementia, 8 mild cognitive impairment, 3 normal control, and 4 patients not suffering from neurodegenerative dementia). Standardized uptake value ratios (SUVRs) were calculated and converted to centiloid (CL) scale to investigate the impact on image quantification. CL pipeline validation were performed to build an equation converting the middle-phase data into equivalent standard scans. Cohen's kappa of binary interpretation and brain amyloid plaque load (BAPL) score were also used to evaluate the intrareader agreement of the FBB image from the two protocols.

Results: The middle-phase FBB SUVR showed an excellent correlation, which provided a linear regression equation of $SUVR_{FBB60-80} = 0.88 \times SUVR_{FBB90-110} + 0.07$, with $R^2=0.98$. The slope of the equation indicated that there was bias between the middle and standard acquisition. This can be converted into the CL scale using $CL = 174.68 \times SUVR - 166.39$. Cohen's kappa of binary interpretation and BAPL score were 1.0 (P<0.0001).

Conclusions: Our findings indicate that the middle-phase FBB protocol is feasible in clinical applications for scans that are at either end of beta-amyloid spectrum, which provides comparable semiquantitative results to standard scan. Patient's waiting time between the injection and scan can be shortened.

Keywords: Florbetaben (FBB); standardized uptake value ratio (SUVR); centiloid (CL); brain amyloid plaque load (BAPL); visual assessment

Introduction

Beta-amyloid positron emission tomography (PET) imaging has become an important technique, as it can serve as a biomarker of Alzheimer's disease (AD). The first beta-amyloid imaging agent was ^{11}C-labeled Pittsburgh compound B (PIB), and was studied in humans by Klunk *et al.* to visualize and measure the deposition of beta-amyloid plaque in the brain (1). However, the short half-life (20 min) of ^{11}C-labeled PIB limits its use in centers with an on-site cyclotron (2). ^{18}F-labeled beta-amyloid imaging agents, such as ^{18}F-florbetapir (AV-45) (3), ^{18}F-florbetaben (FBB) (4), and ^{18}F-flutemetamol (FMM) (5), have a much longer half-life than PIB, which allows the distribution of the tracer to centers without on-site cyclotron. Previous studies proved the uptake of ^{11}C-labeled PIB imaging is highly correlated with that of the ^{18}F-labeled agents (6-8).

There are many studies investigating beta-amyloid imaging quantification (9-20). However, discrepancies in the image analysis methods, different kinetics of the tracers, and highly variable expression of results made it difficult to pool data across multiple sites for comparison among the studies (7). Thus, standardizing the results of beta-amyloid quantification can provide a universal cutoff value and assist in disease diagnosis, observation of disease progression, prognosis, and therapeutic effectiveness (21).

Klunk *et al.* have developed a method to standardize the beta-amyloid quantification by scaling the outcome into the centiloid (CL) scale using PIB images (21). This method allows the conversion of results from a particular analytical method or tracer to a 0-to-100 scale under a rigorous guideline. Previous studies proved that the quantification results of the aforementioned ^{18}F-labeled beta-amyloid tracers can be converted to CL points (7,8,22). The data set and standard volume-of-interest (VOI) are available (Figure S1) on the Global Alzheimer's Association Interactive Network website (GAAIN; https://www.gaain.org/).

FBB is ^{18}F-labeled beta-amyloid tracer commonly used due to its high affinity and specificity to the deposition of beta-amyloid plaque (23,24). Many studies have discussed its application in the CL method, and all of the previous researches used late-phase (scanning from 90 to 110 min after injection) FBB scans to generate beta-amyloid accumulation data (7,25-28). Some researchers focused on early-phase (scanning from 0 to 5 or 10 min after injection) FBB scans, because these scans can indicate cerebral blood flow due to the beta-amyloid tracers' lipophilic property, and they can also serve as a depiction of a perfusion-like image (29-35). Previous work has also investigated on the combination of an early window and late window. These protocols are called dual-phase/dual-time window protocols (36,37). Dual-phase method can reduce the drawback of dynamic scan (long scan time) while maintaining a high quantitative accuracy. In AD, beta-amyloid deposition is abundant in the frontal cortex and can be used to select the optimum imaging time window as suggested in the previous study (38). Some studies revealed that there is an obvious difference in the frontal cortex time-standardized uptake value ratio (SUVR) curve (using the cerebellar cortex as a reference region) between AD patients and healthy controls after 90 min (23,38). Although the SUVR difference is slightly smaller than the time point after 90 min, there is also an obvious discrimination between AD patients and healthy controls at the 60- to 80-min. Therefore, middle-phase (scanning from 60–80 min after injection) FBB scans may be useful for clinical and research applications. However, this type of scanning protocol is seldom used or discussed. Becker *et al.* (11) used 70–90 min interval to calculate the SUVR, and they found SUVR in this interval was excellent in discriminating between beta-amyloid-positive and negative scans, but they did not mention the performance of 60–80 min interval. Another reason for choosing 60–80 min is due to the convenience of clinical setting since 1-hour post-injection provide an easy way to schedule the scan. Other possible time windows could be investigated in future studies.

In this study, we evaluated the feasibility of middle-phase FBB scans using the CL quantification method and the influence on visual assessment using regional cortical tracer uptake (RCTU) and brain amyloid plaque load (BAPL) score. Some AD patients cannot endure the long waiting time of standard FBB protocol (90 min), which would cause the scan failed and increase the cost of hospital. A slightly earlier scanning protocol (middle-phase) while providing comparable results may overcome this situation. By using the middle-phase FBB scans method, the waiting between

4808

Wu et al. Feasibility of middle-phase FBB imaging

Table 1 Subject characteristics

Group	No. of subjects	Gender (male/female)	Age (years)	MMSE score	Middle-phase CL	Standard CL
AD	9	4/5	65±12	16±6	71.92±58.04 (138.99)	70.68±60.74 (135.78)
Mild cognitive impairment	8	3/5	65±6	26±1	−2.67±10.74 (34.00)	−2.45±10.78 (36.87)
Normal control	3	1/2	68±6	29±1	−2.79±6.65 (13.27)	−1.98±3.33 (6.55)
Frontotemporal dementia	2	1/1	74±13	26±2	−17.80±3.86 (5.46)	−14.53±3.12 (4.42)
Dementia with Lewy bodies	1	1/0	64	20	113.61	95.90
Others*	4	0/4	65±3	27±1	52.52±53.64 (119.74)	57.08±53.48 (117.79)

Age and MMSE score are given as mean ± SD. Middle-phase CL and standard CL are given as mean ± SD (maximum – minimum) or mean. *, patients not suffering from neurodegenerative dementia. MMSE, Mini-Mental State Examination; CL, centiloid; AD, Alzheimer's disease; SD, standard deviation.

the injection and scan can be shortened. A more flexible schedule of routine scan for hospital can be acquired since the time from injection to the end of scanning (80 min for middle-phase and 110 min for standard protocol) can be decreased.

Methods

Subject characteristics

Data from 27 subjects (10 men, 17 women) from the Department of Nuclear Medicine, Taipei Veterans General Hospital were collected. Three subjects served as normal controls [68±6 years; Mini-Mental State Examination (MMSE) score: 29±1], and four were patients who did not suffer from neurodegenerative dementia (65±3 years; MMSE score: 27±1). As these four patients had vascular or neurological issues that prevented them from being controls, they are categorized into group "Others" in *Table 1*. The remaining 20 subjects were 9 with AD (65±12 years; MMSE score: 16±6), 8 with mild cognitive impairment (65±6 years; MMSE score: 26±1), 2 with frontotemporal dementia (74±13 years; MMSE score: 26±2), and 1 with dementia with Lewy bodies (64 years; MMSE score: 20). *Table 1* summarizes the subject information. Each subject underwent a middle-phase FBB-PET, a standard FBB-PET, and a T1 magnetic resonance imaging (MRI) scan. This study was conducted in accordance with the Declaration of Helsinki (as revised in 2013). The study was approved by the institutional review board of Taipei Veterans General Hospital (Apr. 27, No. 2021/2021-04-

005AC), and all subjects had provided informed consent.

Image acquisition

All subjects were administered with an intravenous injection of 302.7±23.1 MBq FBB, with FBB acquisition starting 60–80 min after injection (middle-phase FBB). FBB images were acquired on a 3T GE Signa PET/MRI scanner. All images were reconstructed using VPFXS [ordered-subsets expectation maximization (OSEM) with time of flight (TOF) and point spread function (PSF) corrections] algorithm with voxel size 1.17 mm × 1.17 mm × 2.78 mm, and zero echo time (ZTE) magnetic resonance attenuation correction (MRAC) was also applied on the images. At the same time, T1 MRI was acquired under the same scanner. The voxel size was 0.46 mm × 0.46 mm × 1 mm for coronal brain volume (BRAVO) and was 0.46 mm × 0.46 mm × 0.5 mm for axial BRAVO pulse sequence. According to the CL guidelines (21), MRI images were obtained for registration and spatial normalization.

After the middle-phase FBB and T1 MRI scanning, each subject underwent standard FBB-PET scanning on the same day and injection (subjects received only one FBB administration). Standard FBB acquisition started from 90 to 110 min after the same IV injection, which is in accordance with the manufacturer's recommendation and is the same as GAAIN Centiloid Project Database (https://www.gaain.org/centiloid-project). The standard FBB images were acquired on a GE Discovery MI DR PET/computed tomography (CT) scanner. All images were also reconstructed by VPFXS algorithm with a voxel size of

1.17 mm × 1.17 mm × 3.27 mm but with CT attenuation correction (CTAC). These standard FBB images further enabled us to investigate the feasibility of middle-phase FBB images. Although the scanners were different, we still can use an equation to convert the results into CL value (21). The approach of using two scanners may be more patient-friendly and may allow the hospital or clinical site to use the tomograph time-slot for other patients.

CL pipeline validation

The CL pipeline was validated following the criteria specified by Klunk *et al.* (21), detailed description and equations can be found in Appendix 1.

Feasibility of middle-phase FBB SUVR in the CL method

Images from our 27 subjects underwent the same pipeline. We calculated paired standard FBB SUVR and middle-phase FBB SUVR. As noted in the previous section, we can generate the equation:

$$SUVR^{MP-FBB} = m_1 * SUVR^{FBB-Equiv} + b_1 \qquad [1]$$

to convert middle-phase FBB SUVR into equivalent standard FBB SUVR, where $SUVR^{FBB-Equiv}$ represents the equivalent standard FBB SUVR, $SUVR^{MP-FBB}$ represents the middle-phase FBB SUVR, b_1 is the intercept, and m_1 is the slope of linear regression equation. We can further convert it to equivalent PIB SUVR using Eq. [3] and CL using Eq. [2] in Appendix 1. All aforementioned SUVR and CL calculations were performed using MATLAB R2021b (MathWorks Inc., Sherborn, MA, USA).

Visual assessment

In this study, an expert nuclear physician with 10 years of experience in PET amyloid image interpretation evaluated 54 images (27 standard FBB and 27 middle-phase FBB). All DICOM images were anonymized, shuffled, and displayed in the native space. The reader was blinded to clinical information (such as group, age, gender, and MMSE) and imaging protocols (middle-phase FBB or standard FBB). The reader viewed each PET scan via GE AW server 3.2 workstation. PET images were displayed as counts. No other orientation was available (i.e., only displayed in axial view).

The reader used a RCTU scoring system to judge the image. This is the same method as the official guidelines

by life molecular imaging for assessing FBB scans (https://piramal.docebosaas.com/learn). The results of the RCTU were then used for BAPL score to generate the binary interpretation (positive or negative). The detailed RTCU scoring criteria and BAPL score are described in (39).

Statistical analysis

To evaluate the clinical feasibility of the middle-phase FBB image, we must discuss the agreement between the standard FBB and middle-phase FBB image. Paired *t*-test were performed on SUVR and CL. Bland-Altman analysis were conducted on CL. For visual assessment, we calculated the intrareader agreement of binary interpretation and BAPL score between the two protocols using Cohen's kappa, with a significance level of P<0.05.

Results

CL pipeline validation

To validate our local CL pipeline, we calculated the SUVR and converted it to the CL. The linear regression equation between our CL and GAAIN CL was $CL_{site} = CL_{GAAIN} - 0.08$, where $R^2=0.99$ (Figure S2). An excellent correlation was observed, and the pipeline fulfilled CL guideline criteria ($R^2>0.98$, slope 0.98–1.02, and an intercept between −2 and +2). This result indicates that our local CL pipeline is accurate enough to be used.

For converting standard FBB SUVR to CL, paired PIB and FBB SUVRs also showed an excellent correlation, in which $SUVR_{FBB} = 0.61 \times SUVR_{PIB} + 0.39$ with $R^2=0.95$ (Figure S3). This result also fulfills the requirement of the CL guideline ($R^2>0.7$), and the standard FBB image is valid for the CL method. The standard FBB SUVR can be converted to the equivalent PIB SUVR using Eq. [3] in Appendix 1.

Feasibility of middle-phase FBB SUVR in the CL method

Figure 1 shows the distribution of SUVR for standard (90–110 min) FBB and middle-phase (60–80 min) FBB. Paired standard FBB and middle-phase FBB images collected in this study also showed excellent SUVR correlation, which provided a linear regression equation of $SUVR_{FBB60-80} = 0.88 \times SUVR_{FBB90-110} + 0.07$, with $R^2=0.98$ (*Figure 2*), but still there was a significant bias as indicated by the slope. This result also exceeded the minimum

4810

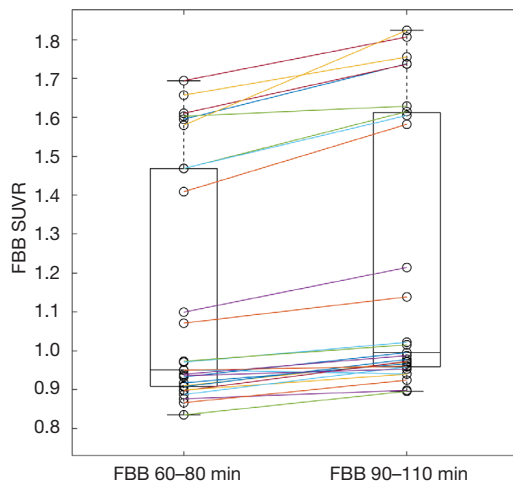Wu et al. Feasibility of middle-phase FBB imaging

Figure 1 Distribution of middle-phase (60–80 min) FBB SUVR and standard (90–110 min) FBB SUVR. FBB, florbetaben; SUVR, standardized uptake value ratio.
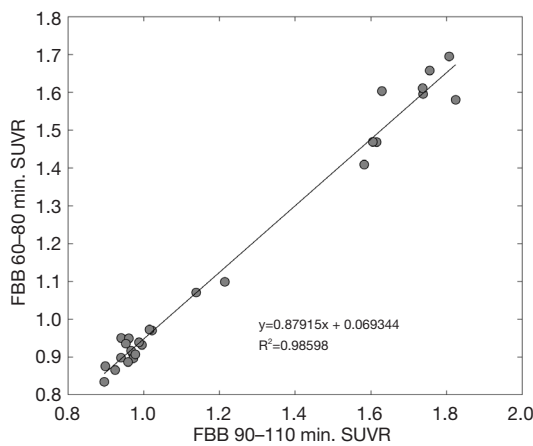

Figure 2 Linear regression between middle-phase (60–80 min) FBB SUVR and standard (90–110 min) FBB SUVR. FBB, florbetaben; SUVR, standardized uptake value ratio.

Table 2 Summary of SUVR and CL of middle-phase and standard FBB image

Protocol	SUVR	CL
Middle-phase FBB	1.14±0.31*	33.54±54.53
Standard FBB	1.22±0.35	33.54±54.14

Data are given as mean ± SD. Paired *t*-test between middle-phase and standard FBB were applied on SUVR and CL, respectively. *, P<0.0001 *vs.* standard FBB. SUVR, standardized uptake value ratio; CL, centiloid; FBB, florbetaben; SD, standard deviation.

Table 3 Equations for converting SUVR into CL

Protocol	Equation
PIB 50–70 min	CL = 93.46 × SUVR – 94.39
FBB 90–110 min	CL = 153.57 × SUVR – 154.27
FBB 60–80 min	CL = 174.68 × SUVR – 166.39

SUVR, standardized uptake value ratio; CL, centiloid; PIB, Pittsburgh compound B; FBB, florbetaben.
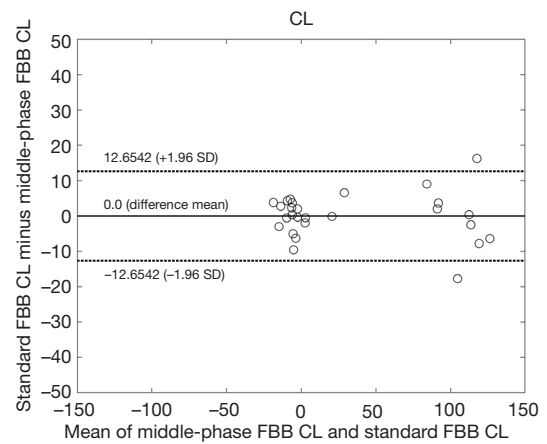

Figure 3 Bland-Altman plot between the middle-phase and standard FBB CL. CL, centiloid; FBB, florbetaben; SD, standard deviation.

acceptance requirement suggested by the CL guideline ($R^2>0.7$). The SUVR of standard and middle-phase scan was 1.22±0.35 and 1.14±0.31, and the corresponding CL was 33.54±54.14 and 33.54±54.53, respectively (*Table 2*). The equation for converting SUVR to CL was CL = 153.57 × SUVR – 154.27 for standard scan, and was CL = 174.68 × SUVR – 166.39 for middle-phase scan (*Table 3*). *Figure 3* displays the agreement between CL converted from middle-phase and standard FBB SUVR using the Bland-Altman plot. The mean difference was very close to 0 (solid line), and most points were located between 12.65 and –12.65 CL unit (dash line).

Statistical analysis

Figure 4A shows the agreement of binary interpretation, and perfect agreement with Cohen's kappa =1 (P<0.0001) was observed. In addition to binary interpretation, the BAPL score also showed perfect agreement, with Cohen's
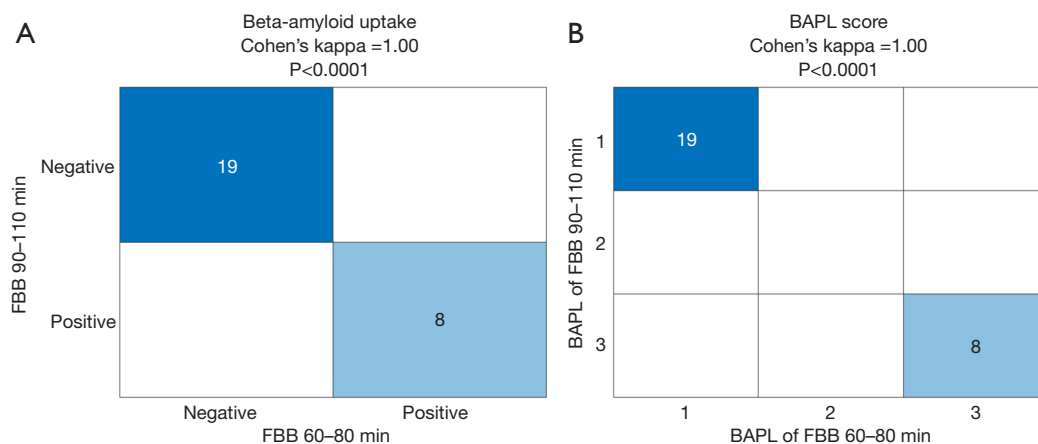
Figure 4 Confusion matrix and Cohen's kappa of visual assessment. (A) Binary interpretation of beta-amyloid uptake; (B) BAPL score. FBB, florbetaben; BAPL, brain amyloid plaque load.

kappa =1 (P<0.0001; *Figure 4B*).

Discussion

The clinical and research applications of middle-phase FBB images were evaluated in this current study. Rather than just applying the results from previous study (7), we recalculated the conversion equation because we omitted the reorientation step. The equation to convert the standard FBB SUVR to PIB SUVR derived by Rowe *et al.* was $SUVR_{FBB} = 0.61 \times SUVR_{PIB} + 0.39$, with $R^2=0.96$, which was very similar to ours: $SUVR_{FBB} = 0.61 \times SUVR_{PIB} + 0.39$, with $R^2=0.95$. The same situation was also found in the equation converting the standard FBB SUVR to CL. The equation derived by Rowe *et al.* was $CL = 153.4 \times SUVR_{FBB} - 154.9$, and our result was $CL = 153.57 \times SUVR_{FBB} - 154.27$. The ratio of standard deviation of FBB and PIB CL in young controls (SD_{FBB}/SD_{PIB}) was 1.98, which was also close to the result conducted by Rowe *et al.* (1.96). This implies that omitting the reorientation step would be fine for the CL method.

With regard to the feasibility of the middle-phase FBB SUVR in the CL method, we found that the middle-phase FBB SUVR fulfilled the CL guideline with a strong correlation ($R^2=0.98>0.7$). Thus, middle-phase FBB SUVR is valid for semiquantitative analysis and can be converted into CL to standardize beta-amyloid imaging measures. Although the correlation is strong, bias as indicated by the slope could also be found. The results need to be validated by applying the equation to convert the middle phase SUVR to CL to another cohort with available middle and standard phase data. This would determine what the resulting bias is in a new cohort at a group and on an individual level. A new FBB imaging protocol that scans from 60 to 80 min after tracer injection may be feasible for research applications. As stated by Klunk *et al.* (21), it remains unclear how differences in scanners, reconstruction algorithms, or methods of attenuation correction might affect the CL value. Rowe *et al.* (7) also indicated that there may be differences between PET systems, and reconstruction methods may have an effect on the use of the conversion equation at other sites. In our study, the middle-phase FBB scans were acquired on a PET/MRI scanner, while standard FBB scans were acquired on a PET/CT scanner. However, we did not collect the same imaging protocol on different scanners; thus, it remains unclear whether equipment-specific equations are needed. Further study may be conducted to uncover the relationship, but this is beyond the scope of this study. Indeed, attenuation correction may not be an issue for the CL method because previous research showed little difference between CTAC and ZTE MRAC (under the same PET/MRI scanner as our study) in the brain region, and accurate attenuation maps can be provided for advanced quantitative brain studies (40). The middle-phase FBB SUVR might be slightly smaller than the standard SUVR and has a narrower dynamic range, and statistical significance was also found in the paired *t*-test. This might be because the different wash-out of radioactivity from both target and reference regions between the two phases (41), and middle-phase SUVR measurement is also prone to be biased by regional cerebral blood flow changes or radiotracer clearance than late scan SUVR (36). Data acquired on different PET scanner may

4812

Wu et al. Feasibility of middle-phase FBB imaging

also introduce some bias between these two measures, and this must be further investigated in future studies. However, we can still convert it to the equivalent standard FBB SUVR using the strongly correlated equation. Moreover, no statistical significance was observed after we converted the SUVR into CL. We also found good agreement (*Figure 3*). The mean difference was very close to 0, and most points were located within the 95% limits of agreement (1.96 SD), strengthening the feasibility of the middle-phase FBB scan for standardizing beta-amyloid imaging quantification and research application. FBB images acquired at other sites can convert their 60- to 80-min FBB SUVR into CL using the equation provided in this study after CL pipeline validation.

The middle-phase FBB protocol also reveals a great agreement with the standard FBB protocol in terms of visual assessment results. Cohen's kappa =1 indicates that the interpretation of the middle-phase FBB is the same as that of standard FBB when judging it as beta-amyloid positive or negative. BAPL score were consistent in each subject. The excellent agreement shown in *Figure 4* could be because only extreme cases were included in the sample, and there are no borderline cases in the gray zone.

However, there are also some limitations in this study. Due to the lack of borderline cases within the gray zone, our findings only hold true for scans that are at either end of the beta-amyloid spectrum (very positive and completely negative). Collecting more borderline data is of importance in future studies. In addition, middle-phase scan is not at pseudoequilibrium state. It has been published that SUVR in early and middle-phase scans are more prone to be biased by regional cerebral blood flow changes than late scans (36,42), which also caused quite a bit of variability between the individual participants CL values in our study (*Figure 3*). The average difference may be 0.0, but for some participants, the difference appears close to 10 or even 15–20 CL, which is a huge difference and not acceptable at an individual level. Differences between the two methods seem to be higher for higher CL values, which would be particularly problematic when using beta-amyloid scans in a clinical setting. Scanning each subject from 60 to 110 min in the same scanner and generating the two imaging windows 60–80 and 90–110 min would allow a more straightforward design and some confounding factors (such as scanner differences, reconstruction, and corrections applied) would have been minimized. Additionally, regulatory issue should be concerned (especially for clinical application) since middle-phase may not be approved by some regulatory authorities such as the European Union, where only 90–110 min is currently supported, even 60–80 min imaging window provides comparable results to late scans (90–110 min).

Collecting more data (especially borderline scan) to verify the equations derived in this study, and minimizing the confounding factors are the focus of the future studies.

Conclusions

The middle-phase FBB protocol is feasible in clinical applications for easy cases (scans that are at either end of beta-amyloid spectrum), especially completely beta-amyloid negative scan, and it can provide comparable semiquantitative results to standard scan. It provides highly correlated results in the standardization of beta-amyloid quantification compared with the standard protocol. Higher CL values (beta-amyloid positive scan) should be paid more attention since a huge CL difference which cannot be acceptable on an individual level may occur. The agreement between the middle-phase and standard protocol was excellent in visual assessment when scoring beta-amyloid deposition. For more difficult cases, whether this protocol would be sufficient should be paid more attention. Using the equations provided in this study after the CL pipeline validation, FBB images acquired at other sites can convert their middle-phase FBB SUVR into CL or build a more robust and less biased equation. The patients' waiting between the injection and scan can be shortened. A more flexible arrangement of routine scan for hospital can be acquired since the time from injection to the end of scanning can be decreased.

Footnote

Conflicts of Interest: All authors have completed the ICMJE uniform disclosure form (available at https://qims.amegroups.com/article/view/10.21037/qims-23-58/coif).

The authors have no conflicts of interest to declare.

Ethical Statement: The authors are accountable for all aspects of the work in ensuring that questions related to the accuracy or integrity of any part of the work are appropriately investigated and resolved. This study was conducted in accordance with the Declaration of Helsinki (as revised in 2013). The study was approved by the institutional review board of Taipei Veterans General Hospital (Apr. 27, No. 2021/2021-04-005AC), and informed consent was obtained from all individual participants included in the study.

References

1. Klunk WE, Engler H, Nordberg A, Wang Y, Blomqvist G, Holt DP, et al. Imaging brain amyloid in Alzheimer's disease with Pittsburgh Compound-B. Ann Neurol 2004;55:306-19.
2. Villemagne VL, Rowe CC. Amyloid PET Ligands for Dementia. PET Clin 2010;5:33-53.
3. Wong DF, Rosenberg PB, Zhou Y, Kumar A, Raymont V, Ravert HT, Dannals RF, Nandi A, Brasić JR, Ye W, Hilton J, Lyketsos C, Kung HF, Joshi AD, Skovronsky DM, Pontecorvo MJ. In vivo imaging of amyloid deposition in Alzheimer disease using the radioligand 18F-AV-45 (florbetapir corrected F 18). J Nucl Med 2010;51:913-20.
4. Barthel H, Gertz HJ, Dresel S, Peters O, Bartenstein P, Buerger K, Hiemeyer F, Wittemer-Rump SM, Seibyl J, Reininger C, Sabri O; Florbetaben Study Group. Cerebral amyloid-β PET with florbetaben (18F) in patients with Alzheimer's disease and healthy controls: a multicentre phase 2 diagnostic study. Lancet Neurol 2011;10:424-35.
5. Rinne JO, Wong DF, Wolk DA, Leinonen V, Arnold SE, Buckley C, Smith A, McLain R, Sherwin PF, Farrar G, Kailajärvi M, Grachev ID. [(18)F]Flutemetamol PET imaging and cortical biopsy histopathology for fibrillar amyloid β detection in living subjects with normal pressure hydrocephalus: pooled analysis of four studies. Acta Neuropathol 2012;124:833-45.
6. Landau SM, Thomas BA, Thurfjell L, Schmidt M, Margolin R, Mintun M, Pontecorvo M, Baker SL, Jagust WJ; Alzheimer's Disease Neuroimaging Initiative. Amyloid PET imaging in Alzheimer's disease: a comparison of three radiotracers. Eur J Nucl Med Mol Imaging 2014;41:1398-407.
7. Rowe CC, Doré V, Jones G, Baxendale D, Mulligan RS, Bullich S, Stephens AW, De Santi S, Masters CL, Dinkelborg L, Villemagne VL. (18)F-Florbetaben PET beta-amyloid binding expressed in Centiloids. Eur J Nucl Med Mol Imaging 2017;44:2053-9.
8. Battle MR, Pillay LC, Lowe VJ, Knopman D, Kemp B, Rowe CC, Doré V, Villemagne VL, Buckley CJ. Centiloid scaling for quantification of brain amyloid with [18F]flutemetamol using multiple processing methods. EJNMMI Res 2018;8:107.
9. Rowe CC, Villemagne VL. Brain amyloid imaging. J Nucl Med 2011;52:1733-40.
10. Thurfjell L, Lundqvist R, Buckley C, Smith A, Sherwin P. Automated quantification of [18F] flutemetamol data-comparison with standard of truth based on histopathology. J Nucl Med 2013;54:302.
11. Becker GA, Ichise M, Barthel H, Luthardt J, Patt M, Seese A, Schultze-Mosgau M, Rohde B, Gertz HJ, Reininger C, Sabri O. PET quantification of 18F-florbetaben binding to β-amyloid deposits in human brains. J Nucl Med 2013;54:723-31.
12. Landau SM, Breault C, Joshi AD, Pontecorvo M, Mathis CA, Jagust WJ, Mintun MA; Alzheimer's Disease Neuroimaging Initiative. Amyloid-β imaging with Pittsburgh compound B and florbetapir: comparing radiotracers and quantification methods. J Nucl Med 2013;54:70-7.
13. Lopresti BJ, Klunk WE, Mathis CA, Hoge JA, Ziolko SK, Lu X, Meltzer CC, Schimmel K, Tsopelas ND, DeKosky ST, Price JC. Simplified quantification of Pittsburgh Compound B amyloid imaging PET studies: a comparative analysis. J Nucl Med 2005;46:1959-72.
14. Tolboom N, Yaqub M, Boellaard R, Luurtsema G, Windhorst AD, Scheltens P, Lammertsma AA, van Berckel BN. Test-retest variability of quantitative [11C]PIB studies in Alzheimer's disease. Eur J Nucl Med Mol Imaging 2009;36:1629-38.
15. Schmidt ME, Chiao P, Klein G, Matthews D, Thurfjell L, Cole PE, Margolin R, Landau S, Foster NL, Mason NS, De Santi S, Suhy J, Koeppe RA, Jagust W; Alzheimer's

Disease Neuroimaging Initiative. The influence of biological and technical factors on quantitative analysis of amyloid PET: Points to consider and recommendations for controlling variability in longitudinal data. Alzheimers Dement 2015;11:1050-68.

16. Villemagne VL, O'Keefe G, Mulligan RS, Rowe CC. Quantitative approaches to amyloid imaging. Methods Mol Biol 2011;680:201-25.

17. Carbonell F, Zijdenbos AP, Charil A, Grand'Maison M, Bedell BJ; Alzheimer's Disease Neuroimaging Initiative. Target Region for Subject Classification on the Basis of Amyloid PET Images. J Nucl Med 2015;56:1351-8.

18. Landau SM, Fero A, Baker SL, Koeppe R, Mintun M, Chen K, Reiman EM, Jagust WJ. Measurement of longitudinal β-amyloid change with 18F-florbetapir PET and standardized uptake value ratios. J Nucl Med 2015;56:567-74.

19. Bullich S, Seibyl J, Catafau AM, Jovalekic A, Koglin N, Barthel H, Sabri O, De Santi S. Optimized classification of (18)F-Florbetaben PET scans as positive and negative using an SUVR quantitative approach and comparison to visual assessment. Neuroimage Clin 2017;15:325-32.

20. Chincarini A, Peira E, Morbelli S, Pardini M, Bauckneht M, Arbizu J, et al. Semi-quantification and grading of amyloid PET: A project of the European Alzheimer's Disease Consortium (EADC). Neuroimage Clin 2019;23:101846.

21. Klunk WE, Koeppe RA, Price JC, Benzinger TL, Devous MD Sr, Jagust WJ, Johnson KA, Mathis CA, Minhas D, Pontecorvo MJ, Rowe CC, Skovronsky DM, Mintun MA. The Centiloid Project: standardizing quantitative amyloid plaque estimation by PET. Alzheimers Dement 2015;11:1-15.e1-4.

22. Navitsky M, Joshi AD, Kennedy I, Klunk WE, Rowe CC, Wong DF, Pontecorvo MJ, Mintun MA, Devous MD Sr. Standardization of amyloid quantitation with florbetapir standardized uptake value ratios to the Centiloid scale. Alzheimers Dement 2018;14:1565-71.

23. Rowe CC, Ackerman U, Browne W, Mulligan R, Pike KL, O'Keefe G, et al. Imaging of amyloid beta in Alzheimer's disease with 18F-BAY94-9172, a novel PET tracer: proof of mechanism. Lancet Neurol 2008;7:129-35.

24. Villemagne VL, Ong K, Mulligan RS, Holl G, Pejoska S, Jones G, O'Keefe G, Ackerman U, Tochon-Danguy H, Chan JG, Reininger CB, Fels L, Putz B, Rohde B, Masters CL, Rowe CC. Amyloid imaging with (18)F-florbetaben in Alzheimer disease and other dementias. J Nucl Med 2011;52:1210-7.

25. Amadoru S, Doré V, McLean CA, Hinton F, Shepherd CE, Halliday GM, Leyton CE, Yates PA, Hodges JR, Masters CL, Villemagne VL, Rowe CC. Comparison of amyloid PET measured in Centiloid units with neuropathological findings in Alzheimer's disease. Alzheimers Res Ther 2020;12:22.

26. Doré V, Bullich S, Rowe CC, Bourgeat P, Konate S, Sabri O, Stephens AW, Barthel H, Fripp J, Masters CL, Dinkelborg L, Salvado O, Villemagne VL, De Santi S. Comparison of (18)F-florbetaben quantification results using the standard Centiloid, MR-based, and MR-less CapAIBL(®) approaches: Validation against histopathology. Alzheimers Dement 2019;15:807-16.

27. Cho SH, Choe YS, Park S, Kim YJ, Kim HJ, Jang H, Kim SJ, Kim JP, Jung YH, Kim BC, Na DL, Moon SH, Seo SW. Appropriate reference region selection of (18)F-florbetaben and (18)F-flutemetamol beta-amyloid PET expressed in Centiloid. Sci Rep 2020;10:14950.

28. Cho SH, Choe YS, Kim HJ, Jang H, Kim Y, Kim SE, Kim SJ, Kim JP, Jung YH, Kim BC, Baker SL, Lockhart SN, Na DL, Park S, Seo SW. A new Centiloid method for (18)F-florbetaben and (18)F-flutemetamol PET without conversion to PiB. Eur J Nucl Med Mol Imaging 2020;47:1938-48.

29. Son SH, Kang K, Ko PW, Lee HW, Lee SW, Ahn BC, Lee J, Yoon U, Jeong SY. Early-Phase 18F-Florbetaben PET as an Alternative Modality for 18F-FDG PET. Clin Nucl Med 2020;45:e8-e14.

30. Daerr S, Brendel M, Zach C, Mille E, Schilling D, Zacherl MJ, Bürger K, Danek A, Pogarell O, Schildan A, Patt M, Barthel H, Sabri O, Bartenstein P, Rominger A. Evaluation of early-phase [18F]-florbetaben PET acquisition in clinical routine cases. Neuroimage Clin 2016;14:77-86.

31. Tiepolt S, Hesse S, Patt M, Luthardt J, Schroeter ML, Hoffmann KT, Weise D, Gertz HJ, Sabri O, Barthel H. Early [(18)F]florbetaben and [(11)C]PiB PET images are a surrogate biomarker of neuronal injury in Alzheimer's disease. Eur J Nucl Med Mol Imaging 2016;43:1700-9.

32. Florek L, Tiepolt S, Schroeter ML, Berrouschot J, Saur D, Hesse S, Jochimsen T, Luthardt J, Sattler B, Patt M, Hoffmann KT, Villringer A, Classen J, Gertz HJ, Sabri O, Barthel H. Dual Time-Point [18F]Florbetaben PET Delivers Dual Biomarker Information in Mild Cognitive Impairment and Alzheimer's Disease. J Alzheimers Dis 2018;66:1105-16.

33. Segovia F, Gómez-Río M, Sánchez-Vañó R, Górriz JM, Ramírez J, Triviño-Ibáñez E, Carnero-Pardo C, Martínez-Lozano MD, Sopena-Novales P. Usefulness of Dual-

Point Amyloid PET Scans in Appropriate Use Criteria: A Multicenter Study. J Alzheimers Dis 2018;65:765-79.

34. Seiffert AP, Gómez-Grande A, Villarejo-Galende A, González-Sánchez M, Bueno H, Gómez EJ, Sánchez-González P. High Correlation of Static First-Minute-Frame (FMF) PET Imaging after 18F-Labeled Amyloid Tracer Injection with [18F] FDG PET Imaging. Sensors (Basel) 2021;21:5182.

35. Yoon HJ, Kim BS, Jeong JH, Kim GH, Park HK, Chun MY, Ha S. Dual-phase (18)F-florbetaben PET provides cerebral perfusion proxy along with beta-amyloid burden in Alzheimer's disease. Neuroimage Clin 2021;31:102773.

36. Bullich S, Barthel H, Koglin N, Becker GA, De Santi S, Jovalekic A, Stephens AW, Sabri O. Validation of Noninvasive Tracer Kinetic Analysis of (18)F-Florbetaben PET Using a Dual-Time-Window Acquisition Protocol. J Nucl Med 2018;59:1104-10.

37. Heeman F, Yaqub M, Lopes Alves I, Heurling K, Berkhof J, Gispert JD, Bullich S, Foley C, Lammertsma AA; AMYPAD Consortium. Optimized dual-time-window protocols for quantitative [18F]flutemetamol and [18F]florbetaben PET studies. EJNMMI Res 2019;9:32.

38. Barthel H, Luthardt J, Becker G, Patt M, Hammerstein E, Hartwig K, Eggers B, Sattler B, Schildan A, Hesse S, Meyer PM, Wolf H, Zimmermann T, Reischl J, Rohde B, Gertz HJ, Reininger C, Sabri O. Individualized quantification of brain β-amyloid burden: results of a proof of mechanism phase 0 florbetaben PET trial in patients with Alzheimer's disease and healthy controls. Eur J Nucl Med Mol Imaging 2011;38:1702-14.

39. Seibyl J, Catafau AM, Barthel H, Ishii K, Rowe CC, Leverenz JB, Ghetti B, Ironside JW, Takao M, Akatsu H, Murayama S, Bullich S, Mueller A, Koglin N, Schulz-Schaeffer WJ, Hoffmann A, Sabbagh MN, Stephens AW, Sabri O. Impact of Training Method on the Robustness of the Visual Assessment of 18F-Florbetaben PET Scans: Results from a Phase-3 Study. J Nucl Med 2016;57:900-6.

40. Sekine T, Ter Voert EE, Warnock G, Buck A, Huellner M, Veit-Haibach P, Delso G. Clinical Evaluation of Zero-Echo-Time Attenuation Correction for Brain 18F-FDG PET/MRI: Comparison with Atlas Attenuation Correction. J Nucl Med 2016;57:1927-32.

41. Cselényi Z, Farde L. Quantification of blood flow-dependent component in estimates of beta-amyloid load obtained using quasi-steady-state standardized uptake value ratio. J Cereb Blood Flow Metab 2015;35:1485-93.

42. Heeman F, Yaqub M, Lopes Alves I, Heurling K, Bullich S, Gispert JD, Boellaard R, Lammertsma AA; AMYPAD Consortium. Simulating the effect of cerebral blood flow changes on regional quantification of [18F]flutemetamol and [18F]florbetaben studies. J Cereb Blood Flow Metab 2021;41:579-89.

Appendix 1

CL pipeline validation

Converting PIB SUVR to CL

To use the CL method, we must confirm that our image analysis pipeline fulfills the CL requirements. We downloaded the PIB and T1 MRI data (34 young controls and 45 AD) from the GAAIN website. Based on the CL guideline (21), a reorientation step is needed that requires reorienting the image so that the coordinate of the anterior commissure is within ~3 cm from the origin and the orientation is within ~15° of the Montreal Neurological Institute (MNI) space. We omitted this tedious process from our study, and just reset the origin as the image center without manually adjusting the anterior commissure-posterior commissure line before image registration. As suggested by the guideline (21), the downloaded MRI images were first registered to the MNI-152 template, and unified segmentation was then applied to the registered MRI images, which, in turn, generated transformation parameters. The downloaded PIB images were registered to the corresponding registered MRI images, and the spatial normalization process was applied to PET images with previously generated transformation parameters. Registration, segmentation, and spatial normalization were completed using SPM8 software (https://www.fil.ion.ucl.ac.uk/spm/). The SUVR was calculated on the spatially normalized PIB image using standard VOIs, which was also downloaded from GAAIN website (as shown in Figure S1). The target region is the global cortical cortex, and the reference region is the whole cerebellum. The PIB SUVR can be converted to CL using the following equation:

$$CL = 100 \times (SUVR_{IND} - SUVR_{YC0})/(SUVR_{AD100} - SUVR_{YC0}) \qquad [2]$$

where $SUVR_{IND}$ represents the individual PIB SUVR, $SUVR_{YC0}$ represents the mean SUVR of 34 young controls, and $SUVR_{AD100}$ represents the mean SUVR of 45 patients with AD. According to the CL guideline, the pipeline accuracy can be validated by plotting the CL calculated by site against the GAAIN CL and calculating the results of linear regression. The percentage error of the average SUVR of AD and young controls between our results and the GAAIN results were within 2% (0.32% for AD, and 0.24% for young controls), and an excellent correlation ($R^2=0.99$) can be observed in the CL pipeline validation section.

Converting standard FBB SUVR to CL

After the pipeline evaluation, we then converted the standard FBB SUVR into the equivalent PIB SUVR or CL using a specific equation. To generate this equation, paired PIB and FBB images were downloaded from the GAAIN website. This data set contained 35 subjects, and detailed subject information can be found in a previous study (7). All images in this data set followed the aforementioned and validated image analysis pipeline; we have also calculated standard FBB and PIB SUVR. By plotting the standard FBB SUVR against the PIB SUVR and calculating the results of linear regression, the conversion equation can be expressed as (standard FBB SUVR) = m_0 × (PIB SUVR) + b_0. Thus, the standard FBB SUVR can be converted into equivalent PIB SUVR by the equation

$$SUVR^{FBB} = m_0 \times SUVR^{PIB-Equiv} + b_0 \qquad [3]$$

where the $SUVR^{PIB-Equiv}$ represents the equivalent PIB SUVR, $SUVR^{FBB}$ represents the standard FBB SUVR, b_0 is the intercept, and m_0 is the slope of the linear regression equation. The standard FBB SUVR can be additionally converted into CL using Eq. [2]. The percentage error of the average FBB and PIB SUVR between our and their results was also within 2% (0.32% for AD $SUVR_{FBB}$, 0.15% for young control $SUVR_{FBB}$, 0.24% for AD $SUVR_{PIB}$, and 0.06% for young control $SUVR_{PIB}$).
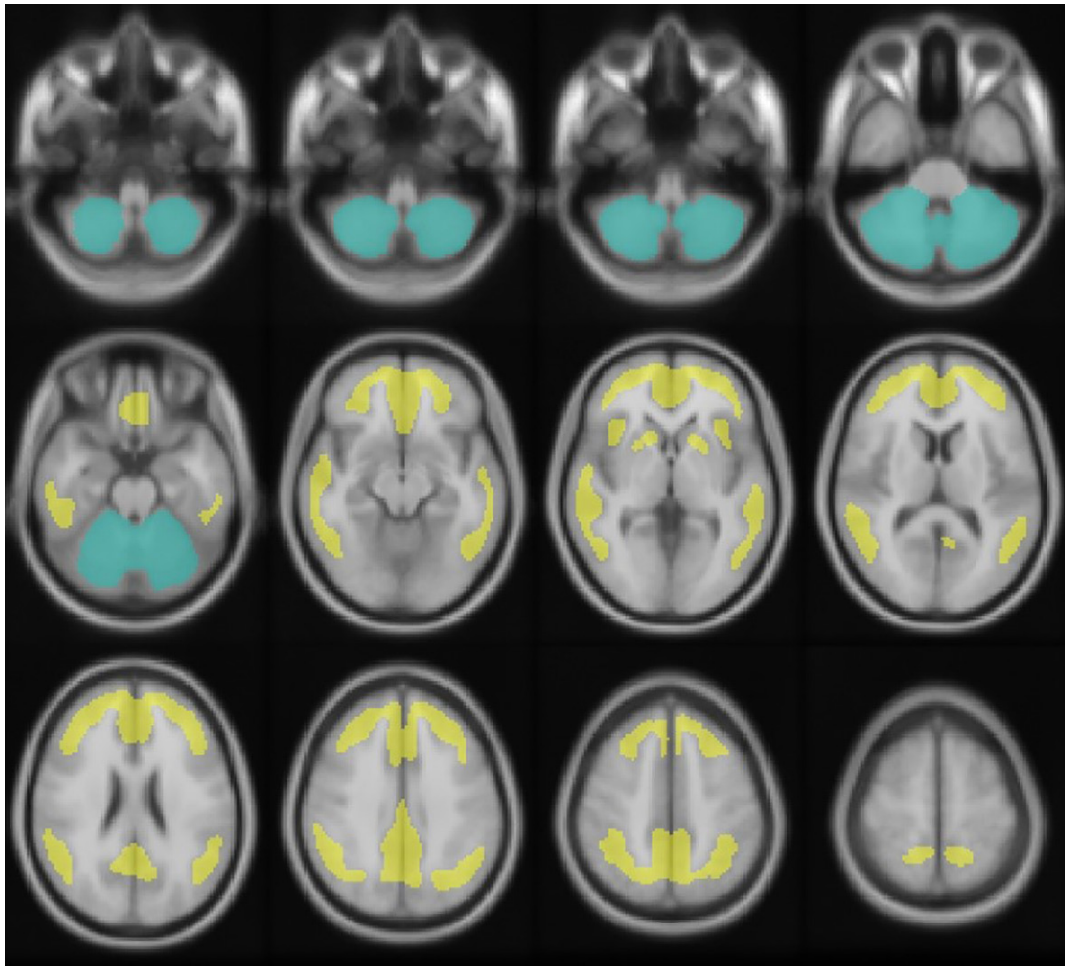
Figure S1 Standard GAAIN volumes-of-interest used for the CL method. The target region (yellow) and reference region (green) are mapped on the MNI-152 template. GAAIN, Global Alzheimer's Association Interactive Network; CL, centiloid; MNI, Montreal Neurological Institute.
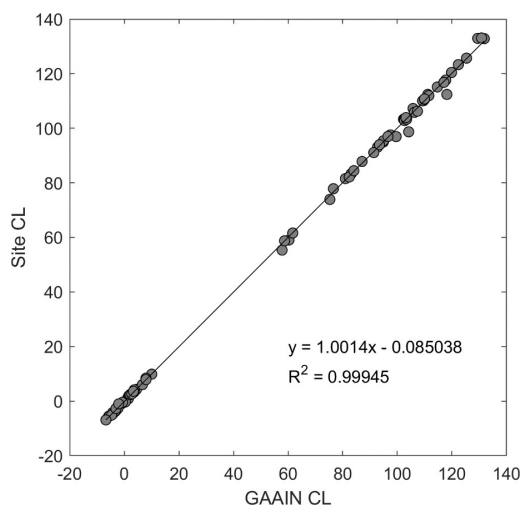

$y = 1.0014x - 0.085038$
$R^2 = 0.99945$

Figure S2 Linear regression between the site CL and GAAIN CL. CL, centiloid; GAAIN, Global Alzheimer's Association Interactive Network.

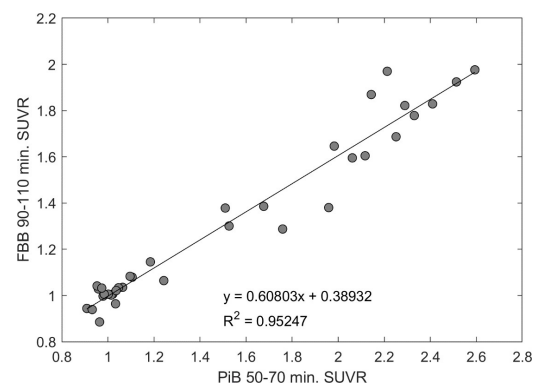$y = 0.60803x + 0.38932$
$R^2 = 0.95247$

Figure S3 Linear regression between FBB SUVR and PIB SUVR. FBB, florbetaben; SUVR, standardized uptake value ratio; PIB, Pittsburgh compound B.